QUANTITATIVE CHARACTERIZATION OF SOOT NANOSTRUCTURE FROM HRTEM IMAGES

M. Moreaud [1], N. Lamharess[2], S. Zinola[2], J. Lavy[2]

1 Technology, Computer Science and Applied Mathematics Division, IFP Energies nouvelles, Solaize, France
2. Energy Application Techniques Division, IFP Energies nouvelles, Solaize, France

ABSTRACT

Diesel particulate filters (DPF) must be periodically regenerated by increasing temperature, typically when a soot load of several grams per liter is deposited. In the recent years, efforts to link structural properties of soot and reactivity have been done to improve DPF regeneration. HRTEM is often used to visualize the soot nanostructure and [1] recently proposed an accurate image analysis method to quantify carbon nanostructure. Our approach is quite similar proposing another noise reduction filter, a completely automatic method of segmentation, a new quantitative characterization not dependent on skeleton calculation method, and a new characterization based on distance between carbon fringes with discrimination between aligned and parallel fringes.

KEYWORDS: distance between objects, HRTEM, segmentation, soot nanostructure.

INTRODUCTION

Diesel particulate matter (DPM) emissions have a significant impact on global climate change by strong absorption of solar radiation in the atmosphere, and on health by penetrating through the human respiratory system. Therefore, DPM emissions are limited since the advent of emission standards for diesel engines in 1993, which have led to generalization of diesel particulate filters (DPF). The exhaust gas is thus forced through porous ceramic channels walls, wherein the particulates are trapped. To avoid increasing fuel consumption and clogging, the DPF must be periodically regenerated by increasing temperature, typically when a soot load of several grams per liter is deposited. In the recent years, efforts to link the chemical, physical and structural properties with the reactivity have been done in order to improve DPF regeneration. High-resolution transmission electron microscopy (HRTEM) is often used to visualize the soot nanostructure but image analysis method to correlate the soot reactivity with the soot nanostructure is always under development. As in [1], we propose image segmentation and analysis method for this type of images. We interest in segmentation and analysis of carbon fringes. These methods can be used to compare several types of soot particles (cf. Figure 1) coming from different combustion modes (i.e. HCCI) or fuels (i.e. biodiesel). The resolution of the image is 0.035nm.pixel^{-1} and intensity is stored in 8 bits format.

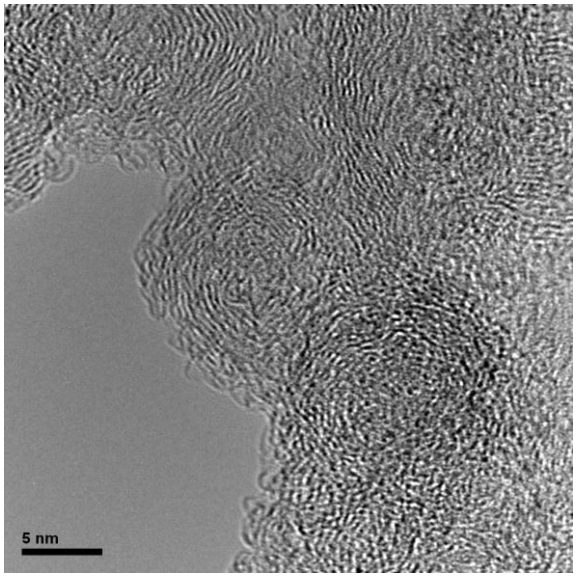

Figure 1: soot HRTEM image (resolution 0.035nm.pixel^{-1}).

SEGMENTATION

Noise reduction

HRTEM images contain electronic noise. As in [2], this noise can be reduced by means of a filter bilateral [3] reducing the noise with very low

impact on strong transitions here corresponding to carbon fringes (cf. Fig. 3). It combines a spatial filter with a filter based on intensity differences. For an image I with spatial support D, the result O of the filter in a voxel x is given by:

$$O(x) = \frac{1}{k(x)} \sum_{y \in D} f(x-y) g(I(x)-I(y)) I(x)$$
$$k(x) = \sum_{y \in D} f(x-y) g(I(x)-I(y))$$

A right choice for f and g is Tukey bi-square function which is statistically more robust to noise than common slow extinction functions as Gaussian function for instance [4]:

$$f(x) = \begin{cases} \frac{1}{2}\left[1-\left(\frac{x}{\sigma_f}\right)^2\right]^2 & |x| \le \sigma_f \\ 0 & \text{otherwise} \end{cases}$$

For g, the expression is the same with parameter σ_g. We use σ_f=1Å and σ_g=30.

Diffraction artifacts removal

Diffraction artifacts (thick white stripes) are localized at the edges of carbon fringes. As in [2], an opening by reconstruction with a disc can be used to remove them [5] (cf. Fig. 3). Assuming O is the result image and I the initial image, we have:

$$O = \gamma^I_{rec}(\varepsilon_{1.5}(I))$$

with $\varepsilon_{1.5}(I)$ morphological erosion with a disc of diameter 1.5Å and $\gamma^A_{rec}(B)$ opening by reconstruction of B in A.

Carbon fringes extraction

For a bright field TEM image, the intensity of a pixel depends on the atomic composition of the observed element and on the local density [6]. Soot's samples containing only carbon, pixels' intensity depends only of the local density of carbon (the higher density, the lower intensity). Carbon fringes consisting of organized carbon atoms are more dense than carbon atoms in amorphous from. Carbon fringes oriented with the same axis as the electron beam appears in the image with very low intensity depending on local thickness of the sample. The carbon fringes extraction can be performed by means of an operator that can extract objects darker than its immediate neighbourhood. We propose to use a Black Top Hat operator [5] with a disc as structuring element (cf. Fig. 3). The diameter of the disc should be a little larger than the higher carbon fringes' thickness (in the present case, 2.5Å). The segmentation threshold s_o of the residue of the opening is estimated by maximizing the interclass variance [7]. Assuming O is the result image and I the initial image, we have:

$$O(x)=I'(x) \mid I'(x)>s_o \text{ with } I'=I-\gamma_{2.5}(I)$$

ANALYSIS

End points extraction

For characterize carbon fringes, we need to know for each fringe the positions of the two end points (i.e. the two farthest points, in the geodesic point of view, contained into the fringe). These points can be extracted from binary image by means of constrained distance map propagated from markers. For distance map, we use an algorithm from [8] ensuring fast execution by the use of hierarchical queue. It includes a sort of tagged pixels to exclude obsolete distances and avoiding duplication of the calculation of local distances. We denote $d_A(I)$ the constrained distance map in I from markers A.

From a set p of points taken randomly in each fringe (one point by fringe), fringes corresponding to connected component $C_x[I]$ of I, the first set of end points p_1 is given by (cf. Fig. 2):

$$p_1 = x \left| \max_{C_x[I]} d_p(I) \right.$$

The second set of end points p_2 is obtained from p_1 (cf. Fig. 2):

$$p_2 = x \left| \max_{C_x[I]} d_{p_1}(I) \right.$$

With this method, there may be several pairs of end points in a single object (as a rectangle, for instance). However, it is very unusual to find this morphology of fringe in practice.

Using the two end points and watershed operator, positions of pseudo centroid c^i of fringe i can be calculated by (cf. Fig. 2):

$$c^i = \bar{x} \,|\, x = W_{dpp}(p_1 \cup p_2), x \in C_i[I] \text{ with } dpp = d_{I_c}(p_1 \cup p_2)$$

and $\bar{x}$ barycenter of set of points x.

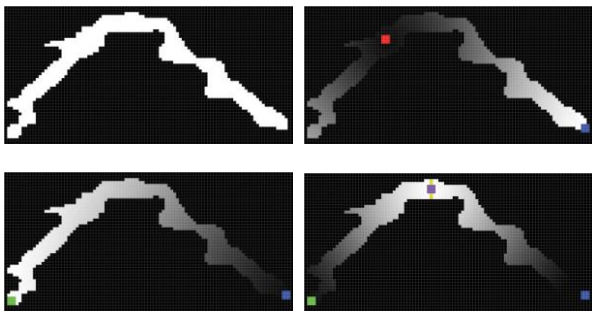

Figure 2: from left to right, and top to bottom: one carbon fringe; random point (red point) and constrained distance propagation from this point: the maximum of the distance gives the first end point (in blue); constrained distance propagation from the first end point: the maximum of the distance gives the second end point (in green); constrained distance propagation from the two end points and watershed line (in yellow): the barycenter of points on watershed line gives the pseudo centroid (in purple).

Fringes morphology characterization

Geodesic length l_g^i of fringe i is obtained from constrained distance map $d_{p1}(I)$ at points p_2. Tortuosity of fringe i is given by the ratio between l_g^i and Euclidean distance between p_1^i and p_2^i. An estimation of mean thickness of a fringe i is given by its surface area divide by l_g^i.

Cleaning

Carbon fringes cut by the limited field of view are removed by a border kill operator [5]. Assuming O the result image, I the initial image, $C_x[I]$ connected components of I, and B border of I, we have:

$$O = C_x[I] \mid C_x[I] \cap B \neq \emptyset.$$

Assuming that carbon fringes with very short geodesic length (<1.5Å) are irrelevant for further analysis. These carbon fringes can be removed by on opening by criteria [9] using geodesic length l as criteria. Assuming O the result image, I the initial image, $C_x[I]$ connected components of I, and l(X) geodesic length of set X, we have:

$$O = \gamma_l(I) = C_x[I] \mid l(C_x[I]) > 1.5Å.$$

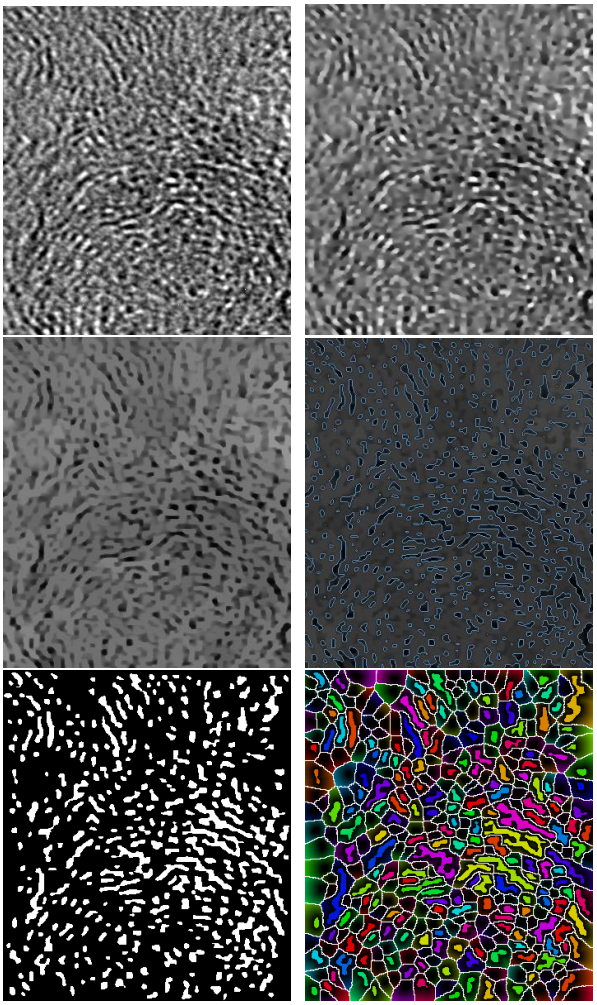

Figure 3: from left to right, and top to bottom: initial image; bilateral filter; diffraction artifacts removal; carbon fringes segmentation; cleaning; distance between fringes (watershed in white and distance in color gradient).

Distance between carbon fringes

Consider a map of the closest neighbors [10] obtained by this way: from a classical distance map, each pixel receiving a local distance is assigned with the coordinates of the source point from which the distance is propagating from. The exact Euclidean distance can be determinate by calculation of Euclidean distance between each pixel and its nearest source point. We denote the map of nearest neighbors of I from A $n_A(I)$, and the corresponding Euclidean distance $d'_A(I)$. If we want to compute distance only with carbon fringes complying a criterion K (such as geodesic length), we can use distance calculation and opening by criteria K. We can define the distance $d'_{i,j}$ between fringes i, j visible from each other by (cf. Fig. 3):

$$d'_{i,j} = \min d'_I\left(I^c\right)(x) \middle| C_i[I] \text{ and } C_j[I] \text{ satify K},$$
$$x \in W_{d'_I(I^c)}(I), \exists (a,b) \in V_x{}^2 \middle| \overrightarrow{n_I(a), x} \wedge \overrightarrow{n_I(b), x} = 0$$

with I^c complementary image of I, V_x immediate neighboring pixels at point x, $W_A(B)$ watershed from markers B on topological function A.

Aligned or parallel carbon fringes discrimination

Using for each carbon fringe i, end points p_1^i and p_2^i, pseudo centroid c^i and distance between fringes, carbon fringes can be discriminated between aligned and parallel fringes. We can model fringes as set of two segments (p_1,c) and (c,p_2) (cf. Fig. 4). For two fringes i and j visible for each other, i.e. $d'_{i,j} \neq \infty$, we can compute four pairs of angles:

$$\cos^{-1}\left(\frac{\overrightarrow{c^i p_a^i}.\overrightarrow{p_a^i p_b^j}}{\left\|\overrightarrow{c^i p_a^i}\right\|\left\|\overrightarrow{p_a^i p_b^j}\right\|}\right) \text{ and } \cos^{-1}\left(\frac{\overrightarrow{p_a^i p_b^j}.\overrightarrow{p_b^j c^j}}{\left\|\overrightarrow{p_a^i p_b^j}\right\|\left\|\overrightarrow{p_b^j c^j}\right\|}\right)$$

with a=1 or 2 and b=1 or 2.

If the two angles of one of these pairs are lower to an angular tolerance α, then we can consider that the two fringes i and j are aligned.

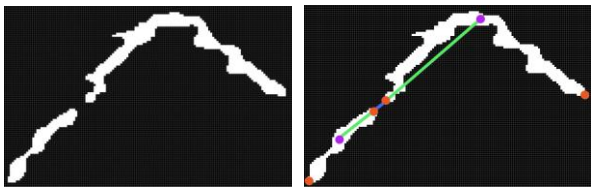

Figure 4: left, two carbon fringes. Right, fringes are modeled with segments (in green) between end points (red points) and pseudo centroids (purple points) to discriminate aligned and parallel fringes.

CONCLUSION

We presented an accurate image segmentation and analysis procedure to characterize carbon fringes of soot on HRTEM images. We proposed denoising and automatic segmentation methods. The proposed characterization method not depends on a skeletonization procedure as in [1]. Moreover, a new characterization method on distance between carbon fringes with discrimination between aligned and parallel fringes is presented. In a future work, some results will be presented on specific soot [11].

REFERENCES

[1] K. Yehliu, R.L. Vander Wal and A.L. Boehman, "A comparison of soot nanostructure obtained using two high resolution transmission electron microscopy image analysis algorithms", Carbon (in press), 2011.

[2] M. Moreaud, R. Revel, D. Jeulin, V. Morard, "Size of boehmite nanoparticles by TEM images analysis", Image Analysis and Stereology, 28, pp. 187-93, 2009.

[3] C. Tomasi, R. Manduchi, "Bilateral filtering for gray and color images", Proc. of International Conference on Computer Vision, IEEE, 1998, pp. 839-46.

[4] M. Black, G. Sapiro, D. Marimont, D. Heeger, "Robust anisotropic diffusion", IEEE Trans. Image Processing 7 3, 1998, pp. 421-32.

[5] J. Serra, "Image analysis and mathematical morphology", Ac. Press, London J, 1982.

[6] P. Hawkes, "The Electron Microscope as a Structure Projector. Electron Tomography, Second Edition Methods for Three-Dimensional Visualization of Structures in the Cell", Joachim Franck, Springer New York, pp. 83-113, 2006.

[7] N. Otsu, "Threshold selection method from gray-level histogram", IEEE Transactions on Systems, Man, and Cybernetics 9 1, pp.62–66, 1979.

[8] L. Ikonen, "Pixel Queue Algorithm for Geodesic Distance Transforms", Berlin, Springer-Verlag, 2005.

[9] T. Walter, "Application de la morphologie mathématique au diagnostic de la rétinopathie diabétique à partir d'images couleur". Thesis, Ecole des Mines de Paris, 2003.

[10] L. Ikonen, "Distance and Nearest Neighbor Transforms of Gray-Level Surfaces Using Priority Pixel Queue Algorithm", Berlin, Springer-Verlag, 2005.

[11] N. Lamharess, C.N. Millet, L. Starck, E. Jeudy, J. Lavy, P. Da Costa, "Catalysed Diesel particulate filter: study of the reactivity of soot arising from biodiesel combustion", Catalysis Today (in press), 2011.

Contact

* M. Moreaud, tel: +33 4 37 70 23 42;
maxime.moreaud@ifpen.fr